Journal Pre-proofs

Construction of Porous g-C_3N_4@PPZ Tubes for High Performance BMI Resin with Enhanced Fire Safety and Toughness

Xia Zhou, Shuilai Qiu, Jiajia Liu, Mutian Zhou, Wei Cai, Junling Wang, Fukai Chu, Weiyi Xing, Lei Song, Yuan Hu

PII: S1385-8947(20)32222-1
DOI: https://doi.org/10.1016/j.cej.2020.126094
Reference: CEJ 126094

To appear in: *Chemical Engineering Journal*

Received Date: 14 January 2020
Revised Date: 23 June 2020
Accepted Date: 24 June 2020

Please cite this article as: X. Zhou, S. Qiu, J. Liu, M. Zhou, W. Cai, J. Wang, F. Chu, W. Xing, L. Song, Y. Hu, Construction of Porous g-C_3N_4@PPZ Tubes for High Performance BMI Resin with Enhanced Fire Safety and Toughness, *Chemical Engineering Journal* (2020), doi: https://doi.org/10.1016/j.cej.2020.126094

This is a PDF file of an article that has undergone enhancements after acceptance, such as the addition of a cover page and metadata, and formatting for readability, but it is not yet the definitive version of record. This version will undergo additional copyediting, typesetting and review before it is published in its final form, but we are providing this version to give early visibility of the article. Please note that, during the production process, errors may be discovered which could affect the content, and all legal disclaimers that apply to the journal pertain.

© 2020 Published by Elsevier B.V.

Construction of Porous g-C_3N_4@PPZ Tubes for High Performance BMI Resin with Enhanced Fire Safety and Toughness

Xia Zhou[a], Shuilai Qiu[a], Jiajia Liu[a], Mutian Zhou[a], Wei Cai[a], Junling Wang[a], Fukai Chu[a], Weiyi Xing [a], Lei Song [a*], and Yuan Hu [a*]

[a]*State Key Laboratory of Fire Science, University of Science and Technology of China, 96 Jinzhai Road, Hefei, Anhui 230026, P.R. China*

Journal Pre-proofs

Corresponding Authors

* Lei Song. Fax/Tel: +86-551-63601642. E-mail: leisong@ustc.edu.cn

* Yuan Hu. Fax/Tel: +86-551-63601664. E-mail: yuanhu@ustc.edu.cn

Abstract

It's acknowledged that the inferior toughness of bismaleimide resin (BMI) is the crucial problem hindering its development and application especially in aerospace, mechanical and electronic fields. While the poor fire safety of toughened BMI is another problem urgently needed to be resolved. Therefore a novel g-C_3N_4@PPZ hierarchical architecture constituted of porous g-C_3N_4 tubes modified by polyphosphazene was designed and fabricated to improve the fire safety and mechanical properties of BMI in this work. Especially compared to pure BMI, the peak heat release rate (PHRR) and peak smoke production rate (PSPR) of BMI with an incorporation of 2 wt% g-C_3N_4@PPZ (BMI/g-C_3N_4@PPZ2.0) are at 246.3 kW/m^2 and 0.12 m^2/s accompanying with 52.1% and 53.8% reduction respectively. The total heat release (THR) and total smoke production (TSP) of BMI/g-C_3N_4@PPZ2.0 are endowed with reductions of 29.4% and 42.9% as well, which demonstrates that the fire safety including heat and smoke hazards of BMI/g-C_3N_4@PPZ2.0 is significantly improved. With regard to the mechanical performance of BMI composites, the impact strength of BMI/g-C_3N_4@PPZ1.5 is 18.89 kJ/m^2 which increases by 184.0% in comparison with that of pure BMI resin (6.65 kJ/m^2). And it's found that the impact strength of BMI/g-C_3N_4@PPZ are still higher than pure BMI in hot-humid environment, which signifies that the BMI/g-C_3N_4@PPZ would be preferred in the industrial applications. Meantime the possible flame retardant and toughening mechanism of g-C_3N_4@PPZ in BMI is detailed investigated and proposed as well.

Key words: Bismaleimide, Polyphosphazene, Toughness, Fire safety, Mechanism

Journal Pre-proofs

1. Introduction.

Bismaleimide (BMI) resin with double active end groups is an important branch of thermosetting polyimide, which can be cross-linked to cure in similar conditions of epoxy resin and unsaturated polyester resin. The bismaleimide which can be as advanced composite matrix, high temperature resistant insulation materials, high temperature resistant structural adhesive, etc. is widely applied in aerospace, transportation and mechanical and electronic fields due to its excellent heat resistance, corrosion resistance, radiation resistance, high mechanical properties. Whereas, the inferior toughness of BMI due to the high degree of crosslinking and benzene ring structures of its main chain is a crucial problem which seriously hinders further developments and applications of BMI.[1, 2] There are many methods of process and toughening modification for BMI, such as aromatic binary amine chain extension modification, allyl compound modification, thermoplastic resin modification, elastomer modification, introduction of new monomer modification, inorganic nano-material modification, etc. Meanwhile, the BD system composed of 4,4-diphenylmethane bismaleimide (BDM) modified by diallyl bisphenol A (DBA) resin has achieved a certain success and been widely used in many resin systems such as XU292 of Ciba-Geigy companies and FM5245, FM5250 of Cytec company in the United States. However, with the modification of toughness reinforcing agents the low fire safety including smoke and heat hazards of BD system becomes another weakness that restricts its further application in industrial fields like electronic fields.[3, 4] Therefore, growing number of studies have been carried out to improve the combination

performance especially the toughness and flame retardant of BD system.[5-13] For example, a PMI-His composed of multi-maleimide terminated branched polysiloxane was obtained to enhance the mechanical and flame retardant properties of BD system.[9] With addition of 15 wt% PMI-HSi, the impact strength of BD system was more than 1.8 times. Meanwhile a functional 3D boron nitride porous framework (sBN) was synthesized to enhance the thermal conductive and flame retardant of BD system as well.[13] The release behavior of heat and smoke of BD/sBN was apparently suppressed. However, to achieve the requested flame retardant and mechanical properties of BMI, the addition amount of designed flame retardants are always relative large. Consequently, it's desired to design an efficient flame retardant and toughening system using various flame retardant and toughening technologies to improve the comprehensive performance of BMI and detailed investigate.[14-16]

Graphite carbon nitride (g-C_3N_4), a two-dimensional layered material, is the most stable allotrope of carbon nitride, which is a poly(tri-triazine) structure composed of nitrogen atoms bridging. Due to the excellent chemical stability, high thermal stability and photoelectric chemical properties of g-C_3N_4, great attentions have been paid to investigate its applications in many fields such as photo-catalysis field, energy field, flame retardant and mechanical enhancer fields in recent years. Especially, the g-C_3N_4 has been widely applied to enhance the flame retardant and mechanical performance of materials due to the advantages of environmental friendliness, abundant component (C, N) elements, low cost, simple large scale preparation and special two-dimensional structure.[17-19] And -NH_2 and -NH groups remained on the surface of g-C_3N_4 are

regarded as active sites to react with other materials containing functional groups, which is another superiority of g-C_3N_4 based hybridization to realize multifunction in composite material system. For example, hybrids of graphitic carbon nitride and organic aluminum hypophosphites (g-C_3N_4/OAHPi) were prepared through esterification and salification reactions, which contributed to reduce the release of heat release and smoke of polystyrene (PS).[20] Therefore it's significant to design a hybridization system based on g-C_3N_4 structure and organics to enhance the toughness and fire safety of BD system.

Cross-linked polyphosphazene, synthesized by nucleophilic substitution of active chlorine in hexachlorocyclotriphosphazene (HCCP), is a typical kind of polyphosphazenes polymers, which is easier to synthesize and has higher yield in comparison with familiar linear polyphosphazenes. Cross-linked polyphosphazenes are widely used to reinforce flame retardant performance of composites due to their high phosphorus and nitrogen contents and high thermal stability.[21-23] Besides, due to the presence of lone pair electrons in phosphorus and nitrogen, the cross-linked polyphosphazene are easy to coordinate with the electrophilic reagents and thus they are effortless to self-assemble on the surface of materials to form a coating layer. Namely, various functional surface modification of fillers can be provided due to the molecular structure designability of the cross-linked polyphosphazenes.[21-25] An amino-rich BP-PZN composed of black phosphorus wrapped by cross-linked polyphosphazene was synthesized and incorporated into epoxy resin, which improved the comprehensive performance including flame retardant and mechanical properties

Journal Pre-proofs

of epoxy.[26] A GNS-Fe_3O_4@PZM consisted of graphene, Fe_3O_4 nanoparticles and cross-linke polyphosphazene was designed to enhance the tribological property of BMI and the aligned GNS-Fe_3O_4@PZM/BMI showed superior thermal stability and mechanical properties as well,[25] which indicates the hybrids of inorganic material and cross-linked polyphosphazene can greatly enhance the comprehensive performance of materials.[25, 26]

As previously mentioned, the toughness and flame retardant properties of BMI are urgent to be improved for exploring its further industrial applications. Hence, based on the toughening principle of inorganic particles toughening and allyl toughening, the g-C_3N_4 nanostructure and cross-linked polyphosphazenes accompanying with molecular designability are utilized in this work to construct a novel BD system equipped with prominent toughness and fire safety, which is supposed to meet industrial production requirements. More precisely, a novel porous tube structure composed of g-C_3N_4 and polyphosphazene (g-C_3N_4@PPZ) is constructed and fabricated. And the porous g-C_3N_4 tube architecture is self-assembled by g-C_3N_4 nanosheets and then is surface modified by a functional cross-linked polyphosphazene designed with allyl functional groups, which is in line with the toughening principles of bismaleimide. Furthermore, the synergistic flame retardant effect of phosphorus-nitrogen elements which compose of the main elements in g-C_3N_4@PPZ is anticipated to greatly improve the fire safety of bismaleimide including low generation of heat and toxic smoke from the combustion. Meanwhile, the mechanisms of mechanical toughening and flame retardant are discussed in detail as well, which is believed to enlighten the further investigation of

bismaleimide composite system.

2. Experimental section.

2.1 Materials.

Hexachlorocyclotriphosphazene (HCCP, 98%) bought from Aladdin Reagent, (China) was purified by recrystallization from n-hexane. Bisphenol-S (BPS 98%), 4,4′-diallyl bisphenol-S (DABPS 98%), dicyandiamide, absolute ethanol were provided by Sinopharm Chemical Reagent Co., Ltd. (China) and used without further treatment. Triethylamine (TEA) and acetonitrile obtained from Aladdin Reagent, China was dehydration using CaH_2. 1,1'-(Methylenedi-4,1-phenylene)bismaleimide (BDM, 98%) and Diallyl bisphenol A (DBA, 90%) were provided by Aladdin Reagent, China as well. Deionized water was obtained from our laboratory.

2.2 Synthesis of 3D porous g-C_3N_4 tubes.

Firstly, 1 g dicyandiamide powders were dissolved in 30 ml deionized water with continuing mechanical stirring for 40 min. Then the solution was diverted to an 80 ml Teflon-lined stainless autoclave and maintained at 180 °C for 5 h. The above solution was following natural cooled to room temperature and then the solution containing dicyandiamide was freeze-dried for about 48 h. Finally the obtained white powders were heated in a ceramic crucible which was put at tube furnace to 600 °C at the 2°C/min and maintained for 4 h. The acquired yellow powders were defined as g-C_3N_4.[27]

2.3 Fabrication of 3D g-C_3N_4@PPZ tubes.

The 3D g-C_3N_4@PPZ tubes were synthesized as followed: the obtained 0.1g g-C_3N_4

and 0.2 g HCCP powders were dispersed in 100 ml acetonitrile accompanying with constant stir and sonication for about 30 min, and this mixture was defined as solution A. Then 0.35 g DABPS, 0.25g BPS and 1.35 ml TEA were diffused in 50 ml acetonitrile with continue stir under sonication for 30 min and defined as solution B. The solution B was next dripped into solution A and this system was reacted at 30 ℃ for 4 h with mechanical stir and sonication. At last the hybrids of g-C_3N_4 and polyphosphazene (PPZ) were collected by centrifugation at 9000 rpm and washed several times utilizing absolute ethanol and deionized water. The final products defined as g-C_3N_4@PPZ were obtained by drying at 80 ℃ for 48 h in vacuum oven.

2.4 Preparation of BMI and BMI/g-C_3N_4@PPZ composites.

The BMI and BMI/g-C_3N_4@PPZ composites were prepared in a typical method. The method of BMI/g-C_3N_4@PPZ1.0 is stated as below. Firstly, 1 g g-C_3N_4@PPZ was included to 42 g of DBA with continue stir and this mixture was maintained at 145 °C for about 30 min. Meantime, 58 g of BDM were melted at 145 °C till the BDM became a transparent and clear liquid. Then the mixture of g-C_3N_4@PPZ and DBA was added into the BDM with further reaction at 145 °C for about 30 min to obtain the pre-polymers. Finally, the pre-polymers was vacuum degassing for another 30 min and thereby the generated polymerized compounds were transferred into preheated mold. The representative curing process of BMI composites was 150 °C/2h + 180 °C/2h + 200 °C/2h + 220 °C/2h + 240 °C/4h and final products were regarded as g-BMI/g-C_3N_4@PPZ1.0 sample. Meanwhile 1 wt% g-C_3N_4@PPZ are replaced by the other proportional amount g-C_3N_4@PPZ additives and the other BMI samples were prepared

in an analogously process.

3. Results and discussion.

3.1 Characterization of g-C_3N_4@PPZ

The preparation process of 3D porous g-C_3N_4@PPZ tubes is presented in Scheme 1. Firstly the porous g-C_3N_4 tube was synthesized through a common calcination method using dicyandiamide obtained after hydrothermal and freeze-drying treatments as precursor and the reaction is presented in Scheme 1. Then the obtained g-C_3N_4 tubes were surface modified by polyphosphazene containing allyl groups, which can increase the matrix compatibility with bismaleimide and inhibit the agglomeration of g-C_3N_4 tubes caused by the formation of hydrogen bond between amino groups on the surface of g-C_3N_4. The g-C_3N_4@PPZ containing allyl groups participated into the formation of bismaleimide cross-linked networks during curing by diene addition reaction and Diels-Alder reaction, which could enhance the interface compatibility between g-C_3N_4@PPZ and BMI resin (Fig.S1). The morphology of g-C_3N_4 and g-C_3N_4@PPZ was characterized by SEM and TEM (Fig.1). It can be noticed that the 3D g-C_3N_4 tubes are self-assembled by irregular g-C_3N_4 nanosheets and the average length of the tubes is dozens of micron (Fig.1a-b). As displayed in Fig.1c-e and Fig.S2a-f, with modification by polyphosphazene, the surface of g-C_3N_4@PPZ becomes much rougher and there is a coating layer about 70 nm on the surface of 3D g-C_3N_4 tubes. Additionally, according to the results of SEM-EDS mapping, the special P, S elements occur and are equally distributed in the g-C_3N_4@PPZ sample, which also reveals that the surface of g-C_3N_4 was successfully modified by polyphosphazene.

The characterizations of XRD and FT-IR were performed to further define the micro composition and structure of g-C_3N_4@PPZ. It can be observed in Fig.2a that two characteristic peaks located at 2θ = 12.9° and 27.7° appear in bulk C_3N_4 sample due to the in-plane tris-triazine ordered alignment and the interlayer stacking reflection of conjugated aromatic segments, which are attributed to the (100) and (002) diffraction planes.[27] Whereas the diffraction peaks of g-C_3N_4 tubes are similar to that of bulk C_3N_4 and the (002) plane of g-C_3N_4 tubes presents an obvious peak at 2θ = 27.9°, larger than bulk g-C_3N_4 sample, which reveals the stacking distance is decreased.[27, 28] Besides, the diffraction peaks of g-C_3N_4 tubes maintain obvious weaker intensity, which might be as a result of poorer inplanar and interlaminar periodicity. The FT-IR patterns of g-C_3N_4 tubes and g-C_3N_4@PPZ were also analyzed and shown in Fig. 2b. It's observed that the g-C_3N_4 tubes and g-C_3N_4@PPZ possess analogous infrared characteristic absorption peaks. Specifically, the stretching vibration of -OH and -NH groups are at 3000 cm^{-1} to 3500 cm^{-1} and meanwhile the characteristic peaks of CN heterocycles are between 1200 cm^{-1} and 1600 cm^{-1}. Furthermore, the obvious peak at 811 cm^{-1} is due to the vibration of tri-s-triazine units in g-C_3N_4. There are some other apparent peaks arising in the g-C_3N_4@PPZ hybrids as well. The characteristic absorptions at 1152 cm^{-1} and 1105 cm^{-1} are ascribed to O=S=O stretching vibration of the sulfonydiphenol units and P=N stretching vibration of the cyclotriphosphazene structure, respectively. The characteristic peaks at 830 and 663 cm^{-1} are attributed to the C-H in the -C=CH and P-Cl, respectively.[24, 25] And the peak located at 883 cm^{-1} and 952 cm^{-1} are belonging to the typical stretching vibration of P-N and Ar-P-O functional groups. Therefore, it can

be concluded that 3D hierarchical g-C_3N_4@PPZ construction was successfully synthesized based on the mentioned analysis.

XPS characterization was conducted to further investigate the chemical composition and structure of g-C_3N_4@PPZ and the results are analyzed in Fig.2c-f.[29-32] There are typical peaks ascribed to C 1s, N 1s, O 1s of the g-C_3N_4 and g-C_3N_4@PPZ samples in the XPS summary spectra. And the additional characteristic peaks of P 2p, S 2s occur in the survey spectrum of g-C_3N_4@PPZ, which implies that the PPZ are coated on the surface of g-C_3N_4. Meanwhile, the high-resolution XPS spectrum of C 1 s in Fig.S3 is fitted into two typical peaks at 284.8 eV and 288.4 eV which are affiliated to the C=C and C-N=C bonds of pure g-C_3N_4. With regard to g-C_3N_4@PPZ, the high-resolution XPS spectrum of C 1 s in Fig.2f is distributed to three characteristic peaks located at 284.5 eV, 286.7 eV and 285.2 eV, which are defined as C=C, C-N=C and C-C bonds. Additionally, some differences appear in the high-resolution XPS spectra of N 1s of pure g-C_3N_4 and g-C_3N_4@PPZ samples in Fig.2d-e. Specially, the three peaks at 398.7 eV, 399.3 eV and 400.9 eV in Fig.2d are assigned to the C-N=C, N-$(C)_3$ in triazine ring and terminal N-H groups of pure g-C_3N_4, respectively and the proportion of terminal amino groups is 6% (atomic content). While the characteristic C-N=C, N-$(C)_3$ peaks of g-C_3N_4@PPZ are located at 398.1 eV, 398.8 eV in Fig.2e. The peak at 400.7 eV is ascribed to the P=N and the peak at 401.5 eV belonging to the terminal amino groups in g-C_3N_4@PPZ sample is obviously smaller than that of pure g-C_3N_4 which suggests that the terminal amino groups of g-C_3N_4 reacted with PPZ during the surface modification. The high-resolution P 2p XPS spectrum of g-C_3N_4@PPZ is

Journal Pre-proofs

analyzed in Fig.S3 as well. And due to the P=N and P-O groups in polyphosphazene the peaks of P 2p in g-C_3N_4@PPZ are fitted into 134.1 eV and 134.9 eV, respectively, which indicates the successful fabrication of 3D hierarchical g-C_3N_4@PPZ construction.

3.2 Thermal properties analysis

The thermal properties of g-C_3N_4, g-C_3N_4@PPZ and BMI/g-C_3N_4@PPZ composites were studied by TGA characterization under nitrogen atmosphere and the results are presented in Fig.3 and Table S1. And it's a consensus that the temperatures ($T_{5wt\%}$ and T_{max}) of reaching 5 wt% thermal weight loss and maximum thermal weight loss rate are the evaluation indexes of thermal properties of materials.[33-36] The char residue amount at 750 °C of polymer materials is also another key information to analyze the thermal properties of polymer materials.[37, 38] It can be noted in Fig.3a that g-C_3N_4 possesses high thermal stability and $T_{5wt\%}$ of it is at 584.5 °C. And at early phase the weight of g-C_3N_4 is slight increased which is owing to the porous structure of g-C_3N_4 tubes. Moreover, $T_{5wt\%}$ of g-C_3N_4@PPZ is decreased to 440.8 °C due to the earlier degradation of polyphosphazene modifying g-C_3N_4 and the initial degradation temperature of g-C_3N_4@PPZ is 296.2 °C which is still far higher than the polymerization temperature of BMI at 240 °C and matches well with the application of BMI. The char residue of g-C_3N_4@PPZ is 35.9 wt% and while the pure g-C_3N_4 displays a rapid weight loss in the range of 550°C to 700°C due to the decomposition of carbon nitride into $(CN)_2$, N_2 or $(CN)_x^+$ without char remaining[39, 40], which implies that the modification of polyphosphazene promotes char formation of g-C_3N_4@PPZ additives. It can be discovered in Fig.3c-d that the thermal degradation of BMI/g-C_3N_4@PPZ

displays a similar process with pure BMI, which presents a one-step degradation process of BMI at about 400 °C. Specifically, as shown in Fig.3c-d and Table S1, $T_{5wt\%}$ and T_{max} of BMI/g-C_3N_4@PPZ composites become slight lower due to the earlier degradation of the g-C_3N_4@PPZ accelerating the degradation of BMI. The residual char of BMI/g-C_3N_4@PPZ3.0 maintains 49.5 wt%, increasing by 89.6% in comparison with that of pure BMI (26.1 wt%). It can be clearly observed from Fig.3d that the maximum weight loss rate of BMI composites decreases with the increased addition of g-C_3N_4@PPZ, which indicates that the thermal degradation of BMI/g-C_3N_4@PPZ is restrained. The remarkable enhanced yield of char residue of BMI/g-C_3N_4@PPZ was due to the interaction of degradation products of g-C_3N_4@PPZ and BMI resin such as condensation, cyclization, cross-linking and other reactions, which is proved by the TGA results of g-C_3N_4, g-C_3N_4@PPZ analyzed in Fig.3a-b and chemical structure of char residue of BMI/g-C_3N_4@PPZ analyzed in Fig.6. Consequently, it's scientifically concluded that the thermal properties of BMI composites are significantly enhanced with the addition of g-C_3N_4@PPZ.

3.3 The fire safety analysis

The cone calorimeter (cone) based on the oxygen consumption principle can relatively easily measure the release of heat and smoke from burning materials under different thermal radiation fluxes, which has become an ideal test instrument for studying and evaluating the combustion properties of materials.[41] Therefore, the cone tests were carried out to evaluate the fire safety of BMI and BMI/g-C_3N_4@PPZ samples and the results are analyzed in Fig.4, Table S2. It can be clearly found in Fig.4 that the

heat release rate (HRR) and smoke production rate (SPR) of BMI composites are significantly inhibited with the incorporation of g-C_3N_4@PPZ. Specifically speaking, the peak value of heat release rate (PHRR) of BMI/g-C_3N_4@PPZ2.0 is 246.3 kW/m^2 which is the lowest value and with a reduction of 52.1% compared to that of pure BMI (514.6 kW/m^2). Meantime the peak value of smoke production rate (PSPR) of BMI/g-C_3N_4@PPZ2.0 in Fig.4c is 0.12 m^2/s, which is decreased by 53.8% in comparison with pure BMI as well. It's noticed that the PHRR and PSPR of BMI/g-C_3N_4@PPZ3.0 sample are 294.2 kW/m^2 and 0.17 m^2/s respectively, which may be owing to the excessive addition of g-C_3N_4@PPZ with high thermal conduction promotes the further combustion of underlayer BMI.[42] As presented in Fig.4, it's discovered that due to the presence of g-C_3N_4@PPZ, the time reaching the peak heat release rate and the smoke production rate of BMI/g-C_3N_4@PPZ composites are shorten, which indicates that the high thermal conductive g-C_3N_4 fillers would promote the thermal transfer to decrease the time.[43] The total heat release (THR) and total smoke production (TSP) vs time curves of BMI and BMI/g-C_3N_4@PPZ are shown in Fig.4b and Fig.4d. And the THR of BMI/g-C_3N_4@PPZ2.0 values 64.1 MJ/m^2 which is decreased by 29.4% in comparison with that of pure BMI (90.9 MJ/m^2). Similar to the heat release behavior, the smoke release behavior of BMI/g-C_3N_4@PPZ2.0 during combustion is distinctly suppressed and the TSP of BMI/g-C_3N_4@PPZ2.0 reduces by 42.9% compared to that of pure BMI. It's deduced that the fire safety of BMI/g-C_3N_4@PPZ composites is evidently improved based on the cone results, which is in line with original intention of designing g-C_3N_4@PPZ architecture.

3.4 Analysis of condensed phase and gas phase flame retardant mechanism

The possible flame retardant mechanism of g-C_3N_4@PPZ is studied on the basis of analysis generated from condensed and gas phases. The char residue after cone tests were collected and investigated by SEM, Raman, XRD, XPS.[44] It can be clearly found from the digital and SEM images in Fig.5a and Fig.5d the char residue of pure BMI presents a fragile and porous morphology. While with addition of g-C_3N_4@PPZ, the quality of char residue is improved significantly. Especially the char residues of BMI/g-C_3N_4@PPZ1.0 and BMI/g-C_3N_4@PPZ2.0 in Fig.5e-f are more compact and robust, and hold much less holes, which perform as a physical barrier to inhibit the transfer of heat, oxygen and combustible gases between external environment and the internal matrix. The graphitization degree of carbonaceous layer can be estimated by Raman spectra. There are two typical absorptions centered at about 1364 and 1600 cm^{-1} which are ascribed to D and G peaks respectively. The D peak at 1364 cm^{-1} is generally considered to be disordered vibration peak of graphite carbon. The G peak at 1600 cm^{-1} is caused by the in-plane vibration of the sp^2 carbon atom. The I_D/I_G which is defined as the ratio of integral area intensity of D and G bands is used to evaluate the graphitization degree.[45, 46] The lower the I_D/I_G value, the higher the degree of graphitization of the char residual and the greater the barrier effect of the underlying polymer.[45, 46] It can be definitely observed in Fig.5g-i that with the inclusion of g-C_3N_4@PPZ, the I_D/I_G is greatly decreased. And the BMI/g-C_3N_4@PPZ2.0 has the lowest I_D/I_G value of 2.31, which indicates that improved char residues of BMI/g-C_3N_4@PPZ samples play an important role in condensed phase flame retardant effect.

To further investigate the flame retardant mechanism of g-C_3N_4@PPZ, the chemical structure and composition of char residue after combustion of BMI samples were studied by XRD and XPS tests (Fig.6).[47] The XRD pattern of char residues of pure BMI and BMI/g-C_3N_4@PPZ2.0 display a similar tendency in Fig.6a. Especially the broad peak at 24° is ascribed to the (002) characteristic peak of graphite carbon and a smaller peak at about 42° is classified into diffraction of (100) or (101) peak of graphite carbon, which reveals that the composition of char residue is mainly the carbon material.[48] Meanwhile, the XPS test was conducted to explore the chemical composition of residue char. There are common C 1s, N 1s and O 1s in the XPS scan-survey spectra of pure BMI and BMI/g-C_3N_4@PPZ2.0 samples which is accordance with the composition of bismaleimide material. Whereas, in Fig.6b an additional P 2p peak occurs in the char residue of BMI/g-C_3N_4@PPZ due to the addition of polyphosphazene. In Fig.6c, the typical peak at 130.2 eV is assigned to the P-Ph band in triphenylphosphine and triphenyl phosphorus oxychloride.[49] And the peaks at 132.9 eV and 133.7 eV are belonging to P-O bonds of $(C_6H_5)_2P(O)N(CH_3)_2$ compounds and P-O bonds of polyphosphoric acid, phosphoric acid compounds.[50, 51] Moreover the characteristic peaks centered at 134.8 eV and 138.26 eV are attributed to P-N bands, $PCl(C_6H_5)_2$ compound.[52] Therefore, it can be deduced that the amount and graphitization of char residue generated from BMI/g-C_3N_4@PPZ composites are increased due to the participant char formation of aromatic phosphorus compounds, nitrogen-containing organic compounds, and phosphoric acid compounds, which endow the underlying resin with a protective barrier.

TG-IR technique was used to investigate the gas pyrolysis products. Three dimension TG-FTIR spectra and the FTIR spectra of pyrolysis products at different temperatures of pure BMI and BMI/g-C_3N_4@PPZ2.0 are presented in Fig.S4 and Fig.7.[53, 54] The pure BMI resin releases more cracked products during thermal decomposition and while the release mount of cracked flammable products for BMI/g-C_3N_4@PPZ2.0 is much less than that of pure BMI in Fig.S4, which means that the g-C_3N_4@PPZ can effectively inhibit the combustion of BMI resin and is consistent with the cone calorimetry results. The TG-DTG vs temperature curves of BMI and BMI/g-C_3N_4@PPZ2.0 obtained from the TG-FTIR tests are shown in Fig.7a and Table S1, which is accordance with the TGA results. As shown in Fig.7b-c that pure BMI and BMI/g-C_3N_4@PPZ2.0 exhibit similar pyrolysis processes.[3, 55] With regard to pure BMI in Fig.7b, when the temperature reaches $T_{5wt\%}$ at 430 °C, the peaks of 2300-2400 cm^{-1} ascribed to CO_2 absorption is clearly observed. In addition, with the temperature increasing, aromatic compounds (1513 cm^{-1}, 1712 cm^{-1}, 3014 cm^{-1}), aliphatic compounds (867 cm^{-1}, 748 cm^{-1}) and nitrogen-containing compounds (1174 cm^{-1}, 1373 cm^{-1}) begin to appear and the absorption intensities become stronger. The degradation of DBA in BMI main chains produces phenol group compounds (3014 cm^{-1}), and the degradation of the imine ring produces carbonyl compounds (1712 cm^{-1}). As the temperature increases, the release amount of each gas product also increases and when the temperature reaches T_{max} (453 °C), these peaks become very noticeable and then weaker. While as for the TG-IR results of BMI/g-C_3N_4@PPZ2.0 in Fig.7c, the infrared absorption peaks are mainly consistent with pure BMI. Specially the intensity of absorption peaks of CO_2 (2300-

2400 cm^{-1}), aromatic compounds (1513 cm^{-1}), nitrogen-containing compounds (1350 cm^{-1}) and aliphatic compounds (748 cm^{-1}) of BMI/g-C_3N_4@PPZ2.0 sample are weaker than pure BMI, which reveals that with the addition of g-C_3N_4@PPZ aliphatic and aromatic compounds generated from the combustion of BMI are more participated into residue char. Meantime due to the participation of aromatic compounds, much denser and more compact char residue layer of BMI/g-C_3N_4@PPZ is formed to block the heat source thereby further reducing the amount of volatiles generated. Furthermore, there is a change about the absorption intensity of the characteristic peaks at 3014 cm^{-1} and 1712 cm^{-1} which reveals the DBA fragments in BMI/g-C_3N_4@PPZ2.0 are mainly degraded into the phenol group compounds. The peak at 3014 cm^{-1} ascribed to phenol groups is overlapped with the characteristic absorption of amino compounds generated from the degradation of g-C_3N_4.[40] When the temperature increases over 500 °C, the typical peaks at 665 cm^{-1}, 713 cm^{-1} ascribed to the C-H in the -C=CH of g-C_3N_4@PPZ and the peaks at 952 cm^{-1}, 1103 cm^{-1} belonging to the typical stretching vibration of Ar-P-O, P-N bonds appear in the FT-IR spectra of BMI/g-C_3N_4@PPZ. The absorptions at 3096 cm^{-1} and 1298 cm^{-1} occurring at the temperature over 500 °C are attributed to the characteristic peaks of amide or amine compounds and CN heterocycles, which suggests series reactions between g-C_3N_4@PPZ and BMI resin are conducted in the degradation. Therefore it can be deduced from the mentioned analysis that when the temperature increases over 500 °C, the g-C_3N_4@PPZ in BMI/g-C_3N_4@PPZ samples are degraded into NH_3 and phosphoric acid compounds, which react with the decomposition products of BMI and facilitate the aliphatic and aromatic compounds

into crosslinked network of char residue layers. And the free radical trapping effect of phosphorus can further improve the flame retardant effect in gas phase of the BMI/g-C_3N_4@PPZ composites.

The absorption intensity of typical decomposition compounds vs time curves of pure BMI and BMI/g-C_3N_4@PPZ2.0 are presented in Fig.7d-i. It can be found that with inclusion of 2 wt% g-C_3N_4@PPZ the total pyrolysis generations of BMI is remarkably decreased. Meanwhile, compared to pure BMI, the intensity of absorption peak of hydrocarbons at 2966 cm^{-1} in BMI/g-C_3N_4@PPZ2.0 sample is obviously reduced. The characteristic absorption of CO_2 and CO are at about 2345 cm^{-1} and 2191 cm^{-1}, respectively. The production of CO_2 during pyrolysis process of BMI/g-C_3N_4@PPZ is lower and while the production of CO is much the same in comparison with that of pure BMI. What's more, the typical peaks of aromatic and organonitrogen compounds are at 1513 cm^{-1} and 1173 cm^{-1}, respectively. As presented in Fig.7h-i, the intensity of aromatic and organonitrogen compounds of BMI/g-C_3N_4@PPZ2.0 are evidently reduced, which suggests that more aromatic and organonitrogen compounds are participated in the formation of char residue. The yields of aromatic and hydrocarbon compounds regarded as typical volatile flammable compounds of BMI/g-C_3N_4@PPZ2.0 are markedly decreased which is favorable in decreasing release amount of heat. Meantime, the yield of smoke is also decreased due to the less generation of aromatic compounds in gas phase, thus heightening the fire safety.

A possible flame retardant mechanism of g-C_3N_4@PPZ is proposed based on the mentioned analysis of condensed and gas products and described in Schematic 2. It can

be inferred the polyphosphazene in g-C_3N_4@PPZ is conversed to organic and inorganic phosphorus compounds such as phosphoric acid or polyphosphoric acid which can form a non-volatile protective film composed of triphenylphosphine, triphenyl phosphorus oxychloride and etc. on the surface of underlayer BMI to insulate the air. And when the temperature is over 500 °C, g-C_3N_4 is decomposed into amino compounds such as NH_3 which can dilute the generated combustible gases.[40] Furthermore, more nitrogen-containing and phosphorus-containing organic compounds are generated and thereby a carbonaceous structure is formed by chemical bonds such as P-C, P-O, P-N remained in the residual char. Consequently, the char residue is endowed with a physical barrier effect, which can inhibit the transfer of combustible gas, oxygen and heat between the outside and the inner layer of BMI, thereby protecting the underlayer BMI from further combustion. In addition, when the BMI/g-C_3N_4@PPZ is burned, due to the existence of polyphosphazene in g-C_3N_4@PPZ, PO· radicals are formed which can react with H·, HO· radicals in the flame region to suppress the flame and interrupt the chain reaction of combustion.[26] The g-C_3N_4@PPZ also facilitates the aromatic compounds and aliphatic hydrocarbons generated from the thermal decomposition of BMI resin to participate in the carbonization reaction, which endows the char residue with higher graphitization degree and more compact structure (Fig.5-6), thereby further suppresses the transfer of heat and mass between BMI matrix and the combustion zone or the outside environment.

3.5 Mechanical properties analysis of BMI and BMI composites

It's acknowledged that the poor toughness of BMI polymers restricts its application.

Therefore the mechanical properties of BMI samples were investigated by the beam impact and DMA tests and the results are displayed in Fig.8 and Table S3. Especially, the toughness of BMI polymers can be evaluated in some way by the impact strength obtained from the beam impact tests. And the better toughness the higher impact strength. It's clearly observed in Fig.8a that with inclusion of g-C_3N_4@PPZ the impact strengths of BMI samples are increased significantly. In particular, the impact strength of BMI/g-C_3N_4@PPZ1.5 possesses the maximum value of 18.89 kJ/m^2 which is increased by 184.0% in comparison with that of pure BMI resin (6.65 kJ/m^2). With the addition of 2 wt% g-C_3N_4@PPZ, the impact strength of BMI increases to 9.89 kJ/m^2, lower than BMI/g-C_3N_4@PPZ1.5 sample which may be due to the unsatisfied dispersion.[56] The storage modulus (E') and the glass transition temperature (Tg) of BMI samples were studied by DMA test and the results are shown in Fig.8c and Fig.S5. All the BMI samples display similar dynamic mechanical thermodynamic processes. The E' of BMI samples from 50 ℃ to 100 ℃ rapidly decrease, which is mainly due to the secondary transformation of the polymer structures and slow declines interval from 100 ℃ to 250 ℃. When the temperature is over 250 ℃, the E' of BMI samples quickly decline, which is due to the glass transition and softening process of cured BMI. The E' of BMI/g-C_3N_4@PPZ samples slightly decrease in comparison with pure BMI which means that the rigidity of BMI with the addition of g-C_3N_4@PPZ is reduced. Meanwhile among the BMI/g-C_3N_4@PPZ samples, BMI/g-C_3N_4@PPZ1.5 possesses the highest storage modulus value of 3463.86 MPa, which is slightly lower than that of pure BMI (3510.71 MPa). As shown in Fig.S5a, the Tg of BMI samples can be obtained through

the temperature of the peak value of Tanδ. It's found that the Tg of BMI with addition of g-C_3N_4@PPZ were slightly decreased which indicates that g-C_3N_4@PPZ plays a role of plasticization in BMI. Specially, due to the reaction between the double bonds of g-C_3N_4@PPZ and the BMI polymer backbone in Fig.S1, the crosslink density of BMI/g-C_3N_4@PPZ polymer network is reduced and thus the segments are easier to move which is manifested by the decreased Tg of BMI/g-C_3N_4@PPZ samples. The comparison of improvement in impact strength of this work and literatures is shown in Fig.8d. It's evident that the impact strength of BMI with inclusion of 1.5 wt% g-C_3N_4@PPZ is significantly increased to 18.89 kJ/m^2 which is with excellent efficiency compared with other BMI systems. And therefore the designed BMI/g-C_3N_4@PPZ system is believed to give some positive effect in further investigates of toughening BMI.[25, 57-64]

To investigate the damp-heat resistance of the BMI samples, the pure BMI and BMI composites splines were treated according to the standard ISO 4611:2008 and then the toughness of the treated splines were characterized by impact test. As presented in Fig.8b, the impact strength of pure BMI obtained from drying after the damp heat test is reduced to 2.58 kJ/m^2 and whereas the impact strength of pure BMI splines without drying after the damp heat test decreases to 3.73 kJ/m^2, which may be attributed to the generated internal stress even cracks as the result of that BMI resin is swelled and absorbs water. Nevertheless, it's a fact that whether the samples treating by the damp heat test is dry or not, the impact strengths of BMI/g-C_3N_4@PPZ are much better than pure sample, which indicates the toughness of BMI composites with inclusion of g-

C_3N_4@PPZ are obviously enhanced in hygrothermal environment. There is a slight difference in the impact strength between the BMI samples in normal environment and hygrothermal environment. In the damp heat test, the dried or undried BMI/g-C_3N_4@PPZ1.0 sample possesses the highest impact strength values of 5.81 kJ/m^2 and 4.69 kJ/m^2 respectively, which is possibly ascribed to the less damages at the interfaces between g-C_3N_4@PPZ and BMI resin in comparison with BMI/g-C_3N_4@PPZ1.5 and BMI/g-C_3N_4@PPZ2.0.

The impact sections of BMI samples were investigated by SEM characterization and the images are shown in Fig.9. The surface of pure BMI presents a typical brittle fracture morphology and many longitudinal cracks in the surface are resemblance to the flows of streams. The cracks in pure BMI collect and form a stress concentrating center which is the break reason of BMI. While the impact surface of BMI/g-C_3N_4@PPZ1.5 and BMI/g-C_3N_4@PPZ2.0 display entirely different morphology compared to pure BMI in Fig.9b-d. It's noticed that many ductile dimple areas are generated in BMI/g-C_3N_4@PPZ samples, which are conductive to transfer, absorb stress, avoid stress concentration. Furthermore, some aggregations of g-C_3N_4@PPZ in BMI/g-C_3N_4@PPZ2.0 are found in Fig.9c-d which would be the centers of stress accompanying with worse interfacial adhesion and result in reduced impact toughness. Therefore, it's deduced that the designed 3D g-C_3N_4@PPZ hierarchal architecture plays a role as stress concentration absorption points and then consumes the stress by deformation, shear yield or microcracks and crack deflection of 3D g-C_3N_4@PPZ. Besides the designed 3D g-C_3N_4@PPZ hierarchal tubes are liable to deformation, shear

Journal Pre-proofs

yield crack deflection performance.[3, 14, 56, 65] Furthermore, the good dispersion of g-C_3N_4@PPZ and excellent interfacial compatibility with BMI resin are much more beneficial to the transfer of stress and microcracks, and can prevent the propagation of microcracks, thereby further improving the toughness of the BMI/g-C_3N_4@PPZ. When the aggregation of g-C_3N_4@PPZ occurs, the microcracks under stress are easier to develop to macroscopic cracks due to the poor interfacial adhesion and reduced distances between microcracks. Additionally due to the excellent thermal stability, water resistance and good interfacial compatibility properties of designed 3D g-C_3N_4@PPZ tubes, the toughness of BMI/g-C_3N_4@PPZ composites are still much better in comparison with pure BMI in damp heat environment, which is believed to play a role in BMI further application.

4. Conclusion.

In this work, a 3D g-C_3N_4@PPZ architecture with excellent thermal and flame retardant properties was designed and synthesized which was expected to offer a solution of poor toughness and unsatisfactory flame retardancy of BMI. It's definite that the 3D g-C_3N_4@PPZ porous tubes composed of irregular nanosheets was successful fabricated based on the analysis of SEM, TEM, XRD characterizations and so on. The TGA and cone tests were conducted to investigate thermal stability and flame retardant properties of pure BMI and BMI/g-C_3N_4@PPZ composites. With addition of g-C_3N_4@PPZ, the yields of char residue of BMI resin are enhanced. Meanwhile, the PHRR and PSPR of BMI/g-C_3N_4@PPZ2.0 have the lowest value of 246.3 kW/m^2 and 0.12 m^2/s, which are accompanied by reductions of 52.1% and 53.8% in comparison

with pure BMI, respectively. Furthermore, compared to pure BMI, the THR of BMI/g-C_3N_4@PPZ2.0 is 64.1 MJ/m^2 decreasing by 29.4% and the TSP reduces by 42.9% as well. Therefore, it's certificated that the fire safety of BMI/g-C_3N_4@PPZ is greatly enhanced which is consistent with pre-assumed intention. The possible flame retardant mechanism of g-C_3N_4@PPZ was proposed on the basis analysis of condensed and gas phases. A series of chemical reactions took place between the g-C_3N_4@PPZ and BMI resin during combustion, which facilitates aromatic compounds and aliphatic hydrocarbons into the formation of char residue. The phosphorus free radical trapping effect of polyphosphazenes and P-N synergistic flame retardant effect of g-C_3N_4@PPZ inhibit the release of heat and smoke as well. On the other hand, the toughness of BMI resin in the normal and hot-humid environments were studied. Specially, with inclusion of g-C_3N_4@PPZ, the BMI composites are endowed with better toughness. Especially the impact strength of BMI/g-C_3N_4@PPZ1.5 is 18.89 kJ/m^2 which increases by 184.0% in comparison with pure BMI resin (6.65 kJ/m^2). The toughness of BMI samples are reduced in the hot-humid environment and whereas the impact strengths of BMI/g-C_3N_4@PPZ are still higher than pure BMI, which signifies that the BMI/g-C_3N_4@PPZ would be preferred in actual industrial applications.

Journal Pre-proofs

ASSOCIATED CONTENT

Supporting Information

The SEM and TEM images of -C_3N_4, g-C_3N_4@PPZ, XPS of g-C_3N_4, g-C_3N_4@PPZ, TGA of pure PPZ, 3D TG-FTIR and mechanical properties of BMI samples are provided.

ACKNOWLEDGMENTS

The work was financially supported by the National Natural Science Foundation of China (21975239), the National Natural Science Foundation of China (51973203), the National Natural Science Foundation of China (51675502), Youth Innovation Promotion Association CAS (2019448), and Fundamental Research Funds for the Central Universities (WK2320000043).

Notes

The authors declare no competing financial interest.

Journal Pre-proofs

Reference:

1. Gu, A.; Liang, G.; Liang, D.; Ni, M., Bismaleimide/carbon nanotube hybrids for potential aerospace application: I. Static and dynamic mechanical properties. Polymers for Advanced Technologies 2007, 18 (10), 835-840.

2. Iredale, R. J.; Ward, C.; Hamerton, I., Modern advances in bismaleimide resin technology: A 21st century perspective on the chemistry of addition polyimides. Progress in Polymer Science 2017, 69, 1-21.

3. Zhou, X.; Qiu, S.; Cai, W.; Liu, L.; Hou, Y.; Wang, W.; Song, L.; Wang, X.; Hu, Y., Construction of hierarchical MoS_2@TiO_2 structure for the high performance bimaleimide system with excellent fire safety and mechanical properties. Chemical Engineering Journal 2019, 369, 451-462.

4. Liu, T.; Sun, L.; Ou, R.; Fan, Q.; Li, L.; Guo, C.; Liu, Z.; Wang, Q., Flame retardant eugenol-based thiol-ene polymer networks with high mechanical strength and transparency. Chemical Engineering Journal 2019, 368, 359-368.

5. Li, W.; Zhou, B.; Wang, M.; Li, Z.; Ren, R., Silane functionalization of graphene oxide and its use as a reinforcement in bismaleimide composites. Journal of Materials Science 2015, 50 (16), 5402-5410.

6. Liang, W.-J.; Zhao, B.; Zhang, C.-Y.; Jian, R.-K.; Liu, D.-Y.; Liu, Y.-Q., Enhanced flame retardancy of DGEBA epoxy resin with a novel bisphenol-A bridged cyclotriphosphazene. Polymer Degradation and Stability 2017, 144, 292-303.

7. Tang, C.; Yan, H.; Li, S.; Li, M.; Chen, Z., Novel phosphorus-containing polyhedral Oligomeric Silsesquioxane functionalized Graphene oxide: preparation and

Journal Pre-proofs

its performance on the mechanical and flame-retardant properties of Bismaleimide composite. Journal of Polymer Research 2017, 24 (10), 157-189.

8. Tian, C.; Yuan, L.; Liang, G.; Gu, A., High thermal conductivity and flame-retardant phosphorus-free bismaleimide resin composites based on 3D porous boron nitride framework. Journal of Materials Science 2019, 54 (10), 7651-7664.

9. Jiang, Z.; Yuan, L.; Liang, G.; Gu, A., Unique liquid multi-maleimide terminated branched polysiloxane and its flame retarding bismaleimide resin with outstanding thermal and mechanical properties. Polymer Degradation and Stability 2015, 121, 30-41.

10. Li, S.; Yan, H. X.; Feng, S. Y.; Niu, S., Synthesis and characterization of a phosphorus-containing flame retardant with double bonds and its application in bismaleimide resins. Rsc Advances 2015, 5 (123), 101480-101486.

11. Li, S.; Yan, H. X.; Feng, S. Y.; Li, X., Phosphorus-containing flame-retardant bismaleimide resin with high mechanical properties. Polymer Bulletin 2016, 73 (12), 3547-3557.

12. Oktay, B.; Cakmakci, E., DOPO tethered Diels Alder clickable reactive silica nanoparticles for bismaleimide containing flame retardant thiol-ene nanocomposite coatings. Polymer 2017, 131, 132-142.

13. Tian, C. F.; Yuan, L.; Liang, G. Z.; Gu, A. J., High thermal conductivity and flame-retardant phosphorus-free bismaleimide resin composites based on 3D porous boron nitride framework. Journal of Materials Science 2019, 54 (10), 7651-7664.

14. Varano, E.; Zhou, M.; Lanham, S.; Iredale, R. J.; van Duijneveldt, J. S.;

Journal Pre-proofs

Hamerton, I., Developing toughened bismaleimide-clay nanocomposites: Comparing the use of platelet and rod-like nanoclays. Reactive and Functional Polymers 2019, 134, 10-21.

15. Guo, Y.; Chen, F.; Han, Y.; Li, Z.; Liu, X.; Zhou, H.; Zhao, T., High performance fluorinated Bismaleimide-Triazine resin with excellent dielectric properties. Journal of Polymer Research 2017, 25 (2), 27-36.

16. Lin, Q.; Zheng, R.; Tian, P., Preparation and characterization of BMI resin/graphite oxide nanocomposites. Polymer Testing 2010, 29 (5), 537-543.

17. Song, B.; Wang, T.; Wang, L.; Liu, H.; Mai, X.; Wang, X.; Wang, N.; Huang, Y.; Ma, Y.; Lu, Y.; Wujcik, E. K.; Guo, Z., Interfacially reinforced carbon fiber/epoxy composite laminates via in-situ synthesized graphitic carbon nitride (g-C_3N_4). Composites Part B: Engineering 2019, 158, 259-268.

18. Song, B.; Wang, T.; Sun, H.; Liu, H.; Mai, X.; Wang, X.; Wang, L.; Wang, N.; Huang, Y.; Guo, Z., Graphitic carbon nitride (g-C_3N_4) interfacially strengthened carbon fiber epoxy composites. Composites Science and Technology 2018, 167, 515-521.

19. Bellardita, M.; García-López, E. I.; Marcì, G.; Krivtsov, I.; García, J. R.; Palmisano, L., Selective photocatalytic oxidation of aromatic alcohols in water by using P-doped g-C_3N_4. Applied Catalysis B: Environmental 2018, 220, 222-233.

20. Shi, Y. Q.; Yu, B.; Duan, L. J.; Gui, Z.; Wang, B. B.; Hu, Y.; Yuen, R. K. K., Graphitic carbon nitride/phosphorus-rich aluminum phosphinates hybrids as smoke suppressants and flame retardants for polystyrene. Journal of Hazardous Materials 2017,

332, 87-96.

21. Xu, L.; Lei, C.; Xu, R.; Zhang, X.; Zhang, F., Hybridization of α-zirconium phosphate with hexachlorocyclotriphosphazene and its application in the flame retardant poly(vinyl alcohol) composites. Polymer Degradation and Stability 2016, 133, 378-388.

22. Qiu, S.; Ma, C.; Wang, X.; Zhou, X.; Feng, X.; Yuen, R. K. K.; Hu, Y., Melamine-containing polyphosphazene wrapped ammonium polyphosphate: A novel multifunctional organic-inorganic hybrid flame retardant. Journal of Hazardous Materials 2018, 344, 839-848.

23. Zhou, X.; Qiu, S.; Xing, W.; Gangireddy, C. S. R.; Gui, Z.; Hu, Y., Hierarchical Polyphosphazene@Molybdenum Disulfide Hybrid Structure for Enhancing the Flame Retardancy and Mechanical Property of Epoxy Resins. ACS Applied Materials & Interfaces 2017, 9 (34), 29147-29156.

24. Jin, W.; Yuan, L.; Liang, G.; Gu, A., Multifunctional Cyclotriphosphazene/Hexagonal Boron Nitride Hybrids and Their Flame Retarding Bismaleimide Resins with High Thermal Conductivity and Thermal Stability. ACS Applied Materials & Interfaces 2014, 6 (17), 14931-14944.

25. Liu, C.; Yan, H.; Lv, Q.; Li, S.; Niu, S., Enhanced tribological properties of aligned reduced graphene oxide-Fe_3O_4@polyphosphazene/bismaleimides composites. Carbon 2016, 102, 145-153.

26. Qiu, S.; Zhou, Y.; Zhou, X.; Zhang, T.; Wang, C.; Yuen, R. K. K.; Hu, W.; Hu, Y., Air-Stable Polyphosphazene-Functionalized Few-Layer Black Phosphorene

for Flame Retardancy of Epoxy Resins. Small 2019, 15 (10), 1805175-1805188.

27. Wu, M.; Zhang, J.; He, B.-b.; Wang, H.-w.; Wang, R.; Gong, Y.-s., In-situ construction of coral-like porous P-doped g-C_3N_4 tubes with hybrid 1D/2D architecture and high efficient photocatalytic hydrogen evolution. Applied Catalysis B: Environmental 2019, 241, 159-166.

28. Cheng, F. X.; Wang, H. N.; Dong, X. P., The amphoteric properties of g-C_3N_4 nanosheets and fabrication of their relevant heterostructure photocatalysts by an electrostatic re-assembly route. Chemical Communications 2015, 51 (33), 7176-7179.

29. Xu, Y.; He, X.; Zhong, H.; Singh, D. J.; Zhang, L.; Wang, R., Solid salt confinement effect: An effective strategy to fabricate high crystalline polymer carbon nitride for enhanced photocatalytic hydrogen evolution. Applied Catalysis B: Environmental 2019, 246, 349-355.

30. Wu, M.; Gong, Y.; Nie, T.; Zhang, J.; Wang, R.; Wang, H.; He, B., Template-free synthesis of nanocage-like g-C_3N_4 with high surface area and nitrogen defects for enhanced photocatalytic H2 activity. Journal of Materials Chemistry A 2019, 7, 5324-5332

31. Wang, H. H.; Guo, H.; Zhang, N.; Chen, Z. S.; Hu, B. W.; Wang, X. K., Enhanced Photoreduction of U(VI) on C_3N_4 by Cr(VI) and Bisphenol A: ESR, XPS, and EXAFS Investigation. Environmental Science & Technology 2019, 53 (11), 6454-6461.

32. Wang, J.; Wang, J.; Han, L.; Liao, C.; Cai, W.; Kan, Y.; Hu, Y., Fabrication of an anode composed of a N, S co-doped carbon nanotube hollow

Journal Pre-proofs

architecture with CoS_2 confined within: toward Li and Na storage. Nanoscale 2019, 11 (43), 20996-21007.

33. Cai, W.; Hu, Y. X.; Pan, Y.; Zhou, X.; Chu, F. K.; Han, L. F.; Mu, X. W.; Zhuang, Z. Y.; Wang, X.; Xing, W. Y., Self-assembly followed by radical polymerization of ionic liquid for interfacial engineering of black phosphorus nanosheets: Enhancing flame retardancy, toxic gas suppression and mechanical performance of polyurethane. J. Colloid Interface Sci. 2020, 561, 32-45.

34. Cai, W.; Mu, X. W.; Pan, Y.; Li, Z. X.; Wang, J. L.; Zhou, X.; Guo, W. W.; Hu, W. Z.; Song, L.; Hu, Y., Black Phosphorous Nanosheets: A Novel Solar Vapor Generator. Solar Rrl 2020, 4 (4), 1900537-19005349.

35. Shi, Y. Q.; Liu, C.; Liu, L.; Fu, L. B.; Yu, B.; Lv, Y. C.; Yang, F. Q.; Song, P. A., Strengthening, toughing and thermally stable ultra-thin MXene nanosheets/polypropylene nanocomposites via nanoconfinement. Chemical Engineering Journal 2019, 378-390.

36. Shi, Y. Q.; Yu, B.; Zheng, Y. Y.; Yang, J.; Duan, Z. P.; Hu, Y., Design of reduced graphene oxide decorated with DOPO-phosphanomidate for enhanced fire safety of epoxy resin. J. Colloid Interface Sci. 2018, 521, 160-171.

37. Zhang, Y.; Hu, Y.; Wang, J.; Tian, W.; Liew, K. M.; Zhang, Y.; Wang, B., Engineering carbon nanotubes wrapped ammonium polyphosphate for enhancing mechanical and flame retardant properties of poly(butylene succinate). Composites Part A: Applied Science and Manufacturing 2018, 115, 215-227.

38. He, L.; Wang, J.; Wang, B.; Wang, X.; Zhou, X.; Cai, W.; Mu, X.;

Journal Pre-proofs

Hou, Y.; Hu, Y.; Song, L., Large-scale production of simultaneously exfoliated and Functionalized Mxenes as promising flame retardant for polyurethane. Composites Part B: Engineering 2019, 179, 107486-107499.

39. Tragl, S.; Gibson, K.; Glaser, J.; Duppel, V.; Simon, A.; Meyer, H. J., Template assisted formation of micro- and nanotubular carbon nitride materials. Solid State Communications 2007, 141 (9), 529-534.

40. Valery N. Khabashesku, J. L. Z., and John L. Margrave, Powder Synthesis and Characterization of Amorphous Carbon Nitride. Chem. Mater. 2000, 12, 3264-3270.

41. Wang, D.; Feng, X.; Zhang, L.; Li, M.; Liu, M.; Tian, A.; Fu, S., Cyclotriphosphazene-bridged periodic mesoporous organosilica-integrated cellulose nanofiber anisotropic foam with highly flame-retardant and thermally insulating properties. Chemical Engineering Journal 2019, 375, 121933-121943.

42. Wu, B.; Ge, L.; Wu, H.; Wang, X.; Ge, Q.; Miao, J.; Cao, M.; Chen, P.; Xia, R.; Qian, J., Layer-by-Layer Assembled g-C_3N_4 Nanosheets/Cellulose Nanofibers Oriented Membrane-Filler Leading to Enhanced Thermal Conductivity. Advanced Materials Interfaces 2019, 6 (4), 1801406-1801419.

43. Cai, W.; Wang, B.; Liu, L.; Zhou, X.; Chu, F.; Zhan, J.; Hu, Y.; Kan, Y.; Wang, X., An operable platform towards functionalization of chemically inert boron nitride nanosheets for flame retardancy and toxic gas suppression of thermoplastic polyurethane. Composites Part B: Engineering 2019, 178, 107462-107475.

44. Guo, W.; Wang, X.; Gangireddy, C. S. R.; Wang, J.; Pan, Y.; Xing, W.; Song, L.; Hu, Y., Cardanol derived benzoxazine in combination with boron-doped

graphene toward simultaneously improved toughening and flame retardant epoxy composites. Composites Part A: Applied Science and Manufacturing 2019, 116, 13-23.

45. Hou, Y.; Qiu, S.; Hu, Y.; Kundu, C. K.; Gui, Z.; Hu, W., Construction of Bimetallic ZIF-Derived Co-Ni LDHs on the Surfaces of GO or CNTs with a Recyclable Method: Toward Reduced Toxicity of Gaseous Thermal Decomposition Products of Unsaturated Polyester Resin. ACS Appl Mater Interfaces 2018, 10 (21), 18359-18371.

46. Mu, X. W.; Wang, D.; Pan, Y.; Cai, W.; Song, L.; Hu, Y., A facile approach to prepare phosphorus and nitrogen containing macromolecular covalent organic nanosheets for enhancing flame retardancy and mechanical property of epoxy resin. Composites Part B-Engineering 2019, 164, 390-399.

47. Cai, W.; Guo, W.; Pan, Y.; Wang, J.; Mu, X.; Feng, X.; Yuan, B.; Wang, B.; Hu, Y., Polydopamine-bridged synthesis of ternary h-BN@PDA@SnO_2 as nanoenhancers for flame retardant and smoke suppression of epoxy composites. Compos. Pt. A-Appl. Sci. Manuf. 2018, 111, 94-105.

48. Li, Z. Q.; Lu, C. J.; Xia, Z. P.; Zhou, Y.; Luo, Z., X-ray diffraction patterns of graphite and turbostratic carbon. Carbon 2007, 45 (8), 1686-1695.

49. Dietzsch, W.; Stach, J.; Kirmse, R., ESR-Einkristalluntersuchungen an dem Gemischtligand-Nickel(III)-Chelat [Ni(mnt)(Et2dtc)]. Zeitschrift für Chemie 1977, 17 (5), 191-192.

50. By Wayne E. Morgan, W. J. S., Royal G. Albridge, and John R. Van Wazer, π-Bond Feedback Interpreted from the Binding Energy of the “2p” Electrons1 of Phosphorus. Inorganic Chemistry 1971, 10 (5), 926-930.

Journal Pre-proofs

51. Fluck E., W. D., P2p-Bindungsenergien in Phosphor(III)-Verbindungen, Phosphonium salzen und Sauerstoffsäuren des Phosphors. Z. Naturforsch. B 1974, 29, 603-607.

52. Franke, R.; Chassé, T.; Streubel, P.; Meisel, A., Auger parameters and relaxation energies of phosphorus in solid compounds. Journal of Electron Spectroscopy and Related Phenomena 1991, 56 (4), 381-388.

53. Chu, F.; Hou, Y.; Liu, L.; Qiu, S.; Cai, W.; Xu, Z.; Song, L.; Hu, W., Hierarchical Structure: An effective Strategy to Enhance the Mechanical Performance and Fire Safety of Unsaturated Polyester Resin. ACS Appl Mater Interfaces 2019, 11 (32), 29436-29447.

54. Wang, J.; Zhang, D.; Zhang, Y.; Cai, W.; Yao, C.; Hu, Y.; Hu, W., Construction of multifunctional boron nitride nanosheet towards reducing toxic volatiles (CO and HCN) generation and fire hazard of thermoplastic polyurethane. Journal of Hazardous Materials 2019, 362, 482-494.

55. Zhou, X.; Mu, X.; Cai, W.; Wang, J.; Chu, F.; Xu, Z.; Song, L.; Xing, W.; Hu, Y., Design of Hierarchical NiCo-LDH@PZS Hollow Dodecahedron Architecture and Application in High-Performance Epoxy Resin with Excellent Fire Safety. ACS applied materials & interfaces 2019, 11, 41736−41749.

56. Yao, W.; Gu, A.; Liang, G.; Zhuo, D.; Yuan, L., Preparation and properties of hollow silica tubes/bismaleimide/diallylbisphenol A composites with improved toughness, dielectric properties, and flame retardancy. 2012, 23 (3), 326-335.

57. Liu, C.; Yan, H.; Chen, Z.; Yuan, L.; Liu, T., Enhanced tribological properties

Journal Pre-proofs

of bismaleimides filled with aligned graphene nanosheets coated with Fe_3O_4 nanorods. Journal of Materials Chemistry A 2015, 3 (19), 10559-10565.

58. Wang, Y.; Liu, S.; Chen, P.; Zhu, X.; Xia, L., Investigation of the curing mechanism and properties of bismaleimide-triazine resins containing phenolphthalein and cyano group. Journal of Applied Polymer Science 2019, 136 (18), 47420-47426.

59. Liu, C.; Dong, Y.; Lin, Y.; Yan, H.; Zhang, W.; Bao, Y.; Ma, J., Enhanced mechanical and tribological properties of graphene/bismaleimide composites by using reduced graphene oxide with non-covalent functionalization. Composites Part B: Engineering 2019, 165, 491-499.

60. Chen, Z.; Yan, H.; Guo, L.; Li, L.; Yang, P.; Liu, B., A novel polyamide-type cyclophosphazene functionalized rGO/WS_2 nanosheets for bismaleimide resin with enhanced mechanical and tribological properties. Composites Part A: Applied Science and Manufacturing 2019, 121, 18-27.

61. Zhu, Y.; Yuan, L.; Liang, G.; Gu, A., Green flame retarding bismaleimide resin with simultaneously good processing characteristics, high toughness and outstanding thermal stability based on a multi-functional organic boron compound. Polymer Degradation and Stability 2015, 118, 33-44.

62. Guo, Y.; Han, Y.; Liu, F.; Zhou, H.; Chen, F.; Zhao, T., Fluorinated bismaleimide resin with good processability, high toughness, and outstanding dielectric properties. Journal of Applied Polymer Science 2015, 132 (46), 42791-42799.

63. Chen, Z.; Yan, H.; Lyu, Q.; Niu, S.; Tang, C., Ternary hybrid nanoparticles of reduced graphene oxide/graphene-like MoS_2/zirconia as lubricant additives for

Journal Pre-proofs

bismaleimide composites with improved mechanical and tribological properties. Composites Part A: Applied Science and Manufacturing 2017, 101, 98-107.

64. Jena, R. K.; Yue, C. Y.; Sk, M. M.; Ghosh, K., A novel high performance bismaleimide/diallyl bisphenol A (BMI/DBA)–epoxy interpenetrating network resin for rigid riser application. RSC Advances 2015, 5 (97), 79888-79897.

65. Chen, Z.; Yan, H.; Liu, T.; Niu, S., Nanosheets of MoS_2 and reduced graphene oxide as hybrid fillers improved the mechanical and tribological properties of bismaleimide composites. Composites Science and Technology 2016, 125, 47-54.

Journal Pre-proofs

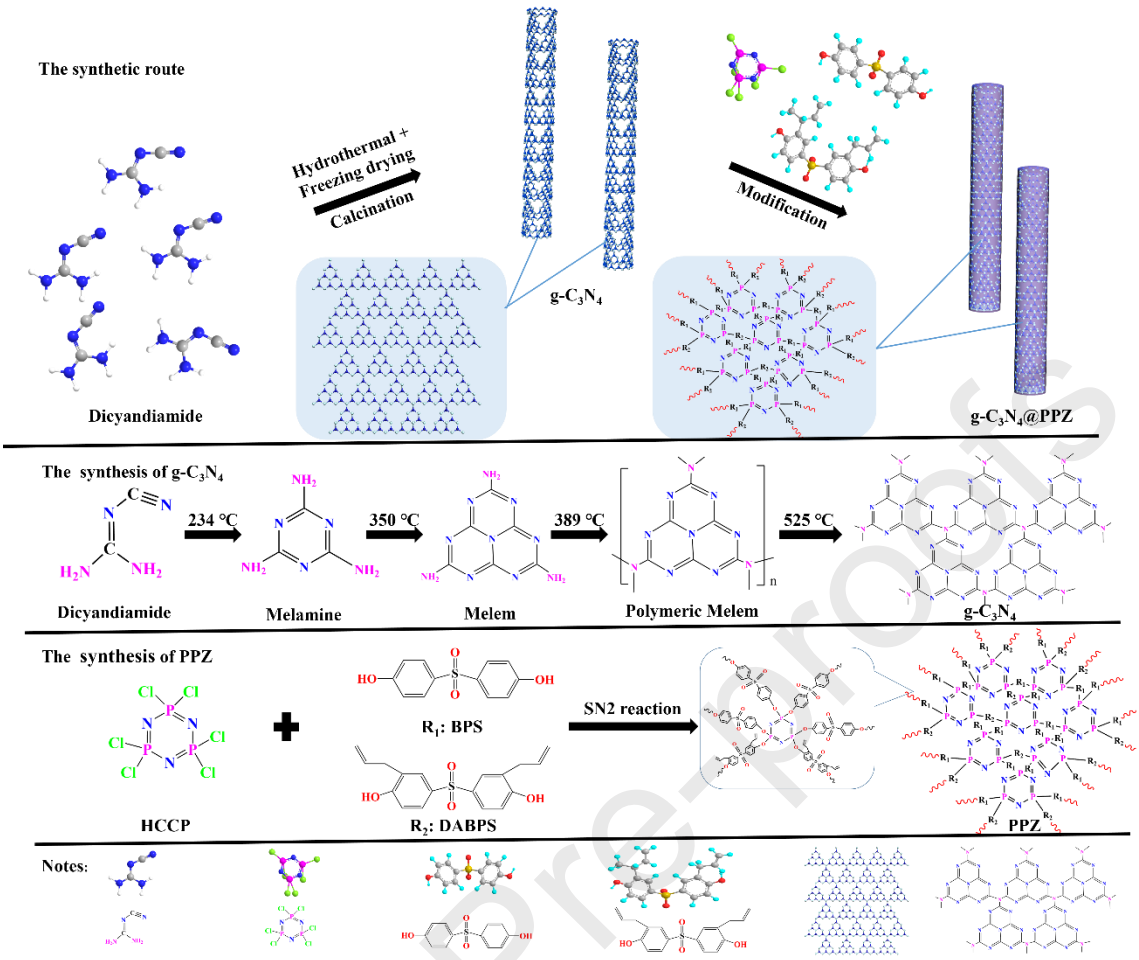

Scheme 1. Schematic diagram of the synthetic route of g-C_3N_4@PPZ.

Journal Pre-proofs

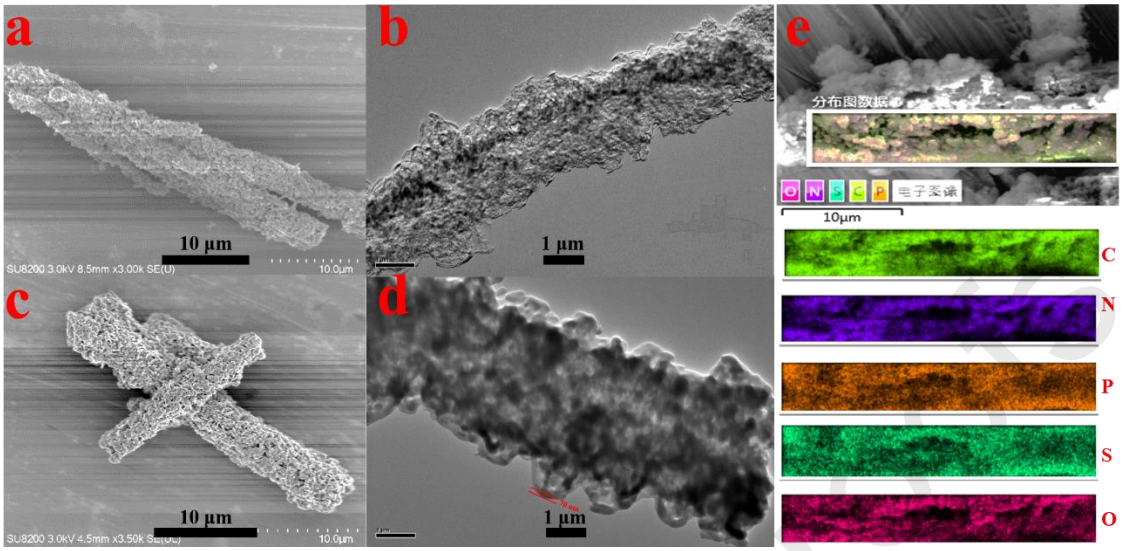

Fig.1 The SEM and TEM images of pure g-C_3N_4 (a-b), g-C_3N_4@PPZ (c-d), and SEM mapping results of g-C_3N_4@PPZ (e).

Journal Pre-proofs

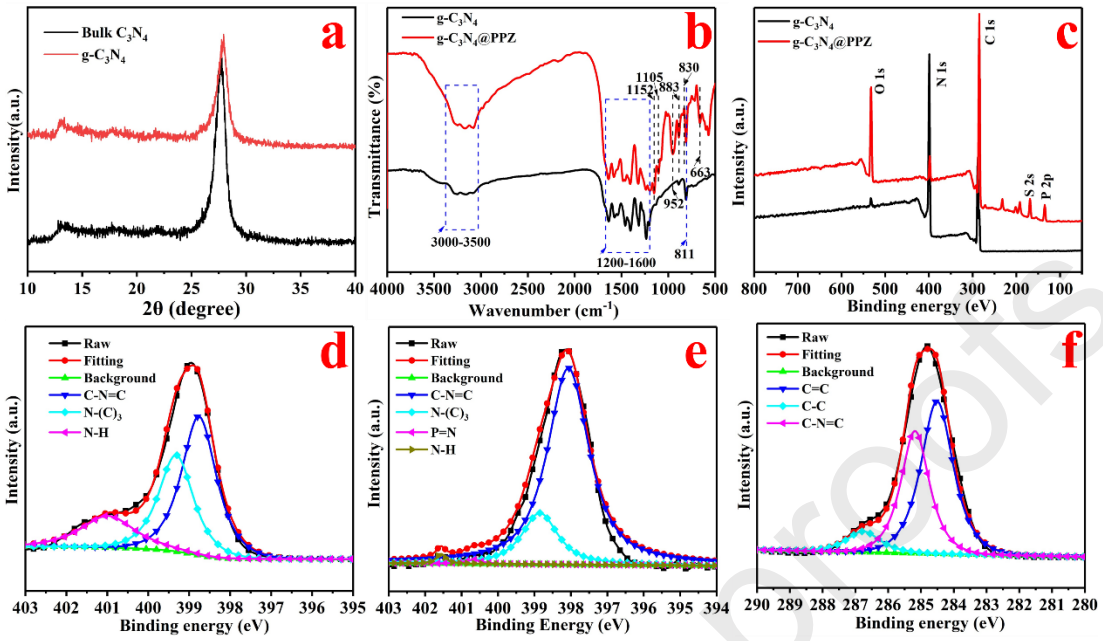

Fig.2 XRD patterns of bulk C_3N_4 and g-C_3N_4 (a); FT-IR spectra (b) and XPS survey spectra (c) of g-C_3N_4 and g-C_3N_4@PPZ; high-resolution N 1s XPS spectra of of g-C_3N_4 (d) and g-C_3N_4@PPZ (e) and high-resolution C 1s XPS spectrum of g-C_3N_4@PPZ (f).

Journal Pre-proofs

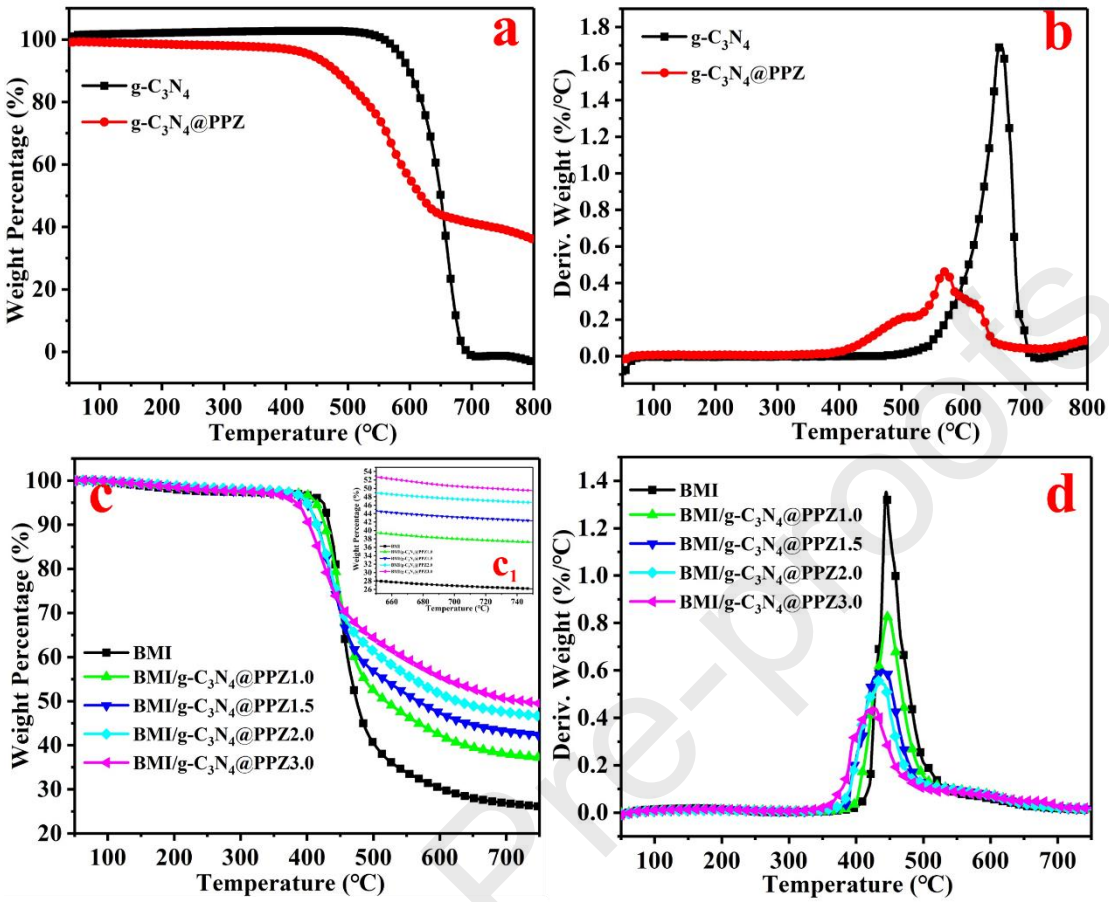

Fig.3 The TGA curves and DTG curves of g-C_3N_4, g-C_3N_4@PPZ in N_2 atmosphere (a-b); the TGA curves and DTG curves of pure BMI and BMI composites (c-d).

Journal Pre-proofs

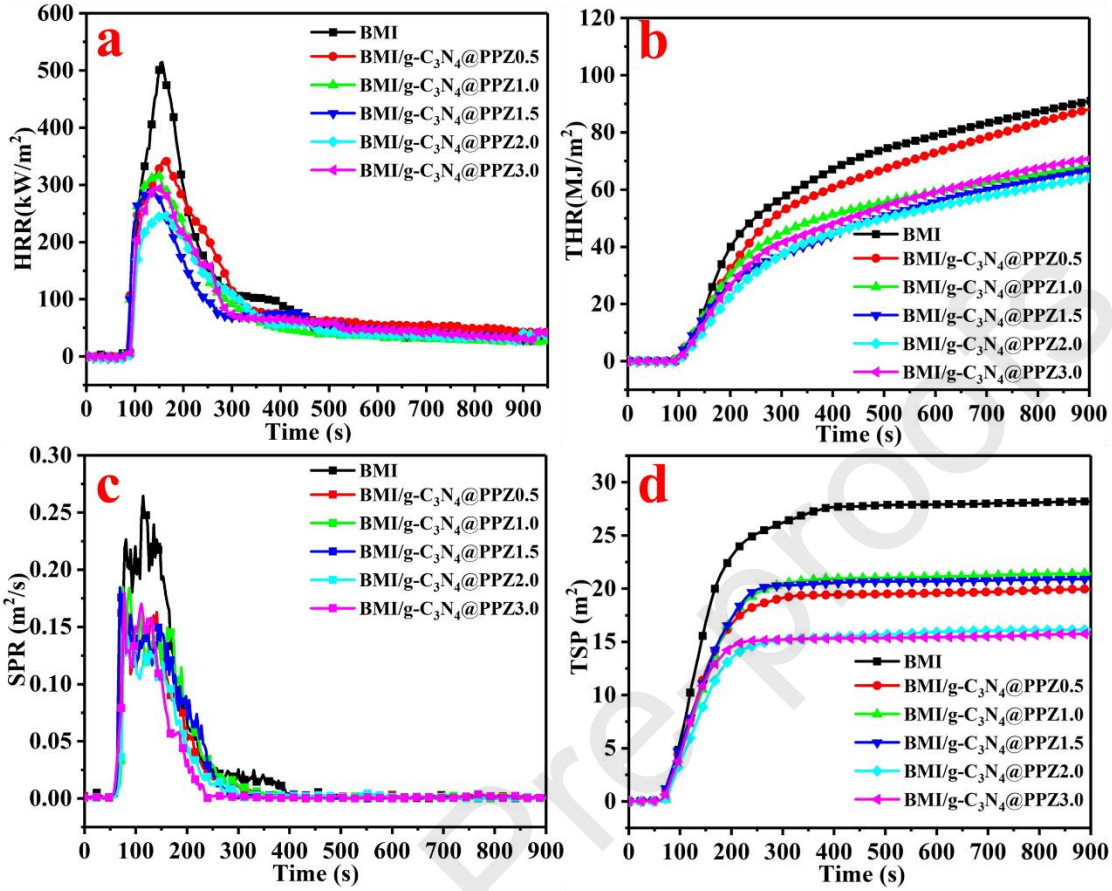

Fig.4 The heat release rate (HRR), smoke production rate (SPR), total heat release (THR) and total smoke production (TSP) vs time curves of BMI and BMI composites (a-d).

Journal Pre-proofs

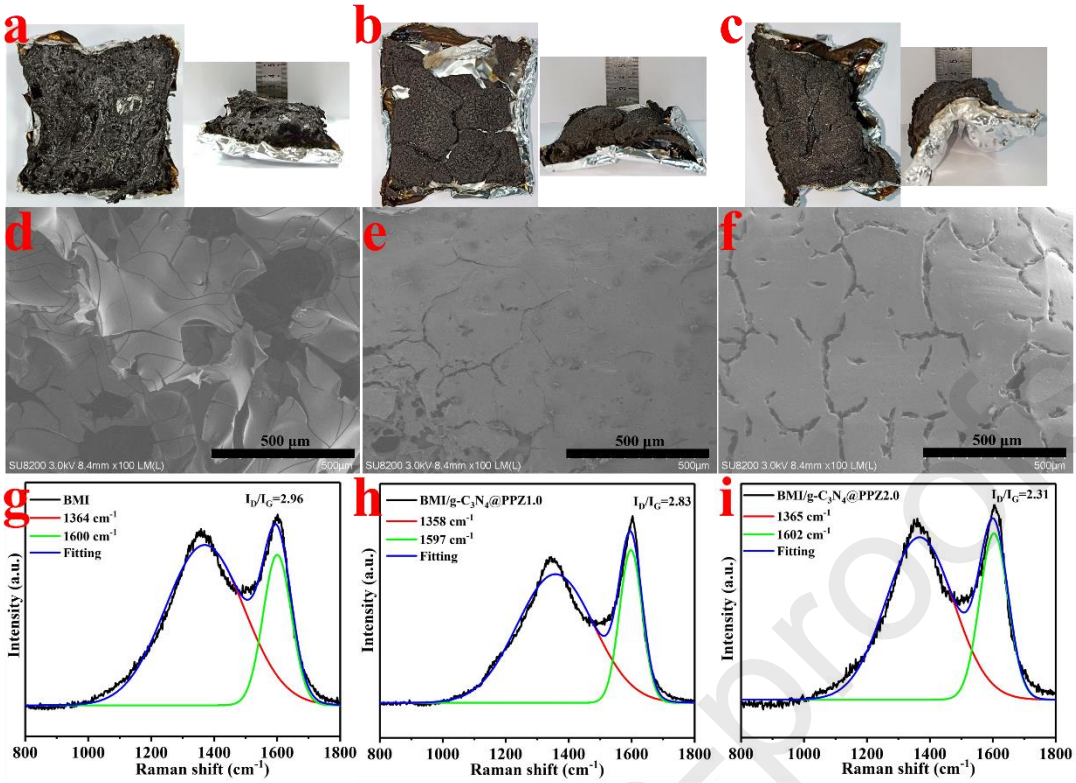

Fig.5 The digital photos of the residue char of pure BMI, BMI/g-C_3N_4@PPZ1.0 and BMI/g-C_3N_4@PPZ2.0 after cone test from top view and side view (a-c); the SEM images and Raman spectra of the residue char of pure BMI, BMI/g-C_3N_4@PPZ1.0 and BMI/g-C_3N_4@PPZ2.0 (d-i).

Journal Pre-proofs

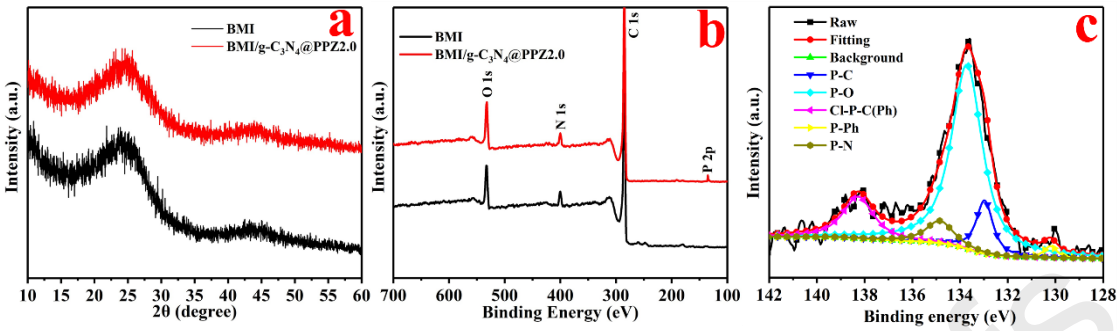

Fig.6 XRD patterns for the char residue of pure BMI, BMI/g-C_3N_4@PPZ2.0 after cone tests (a); XPS survey spectra for the residual char of pure BMI, BMI/g-C_3N_4@PPZ2.0 (b) and the high-resolution P2p XPS spectrum for the residual char of BMI/g-C_3N_4@PPZ2.0 (c).

Journal Pre-proofs

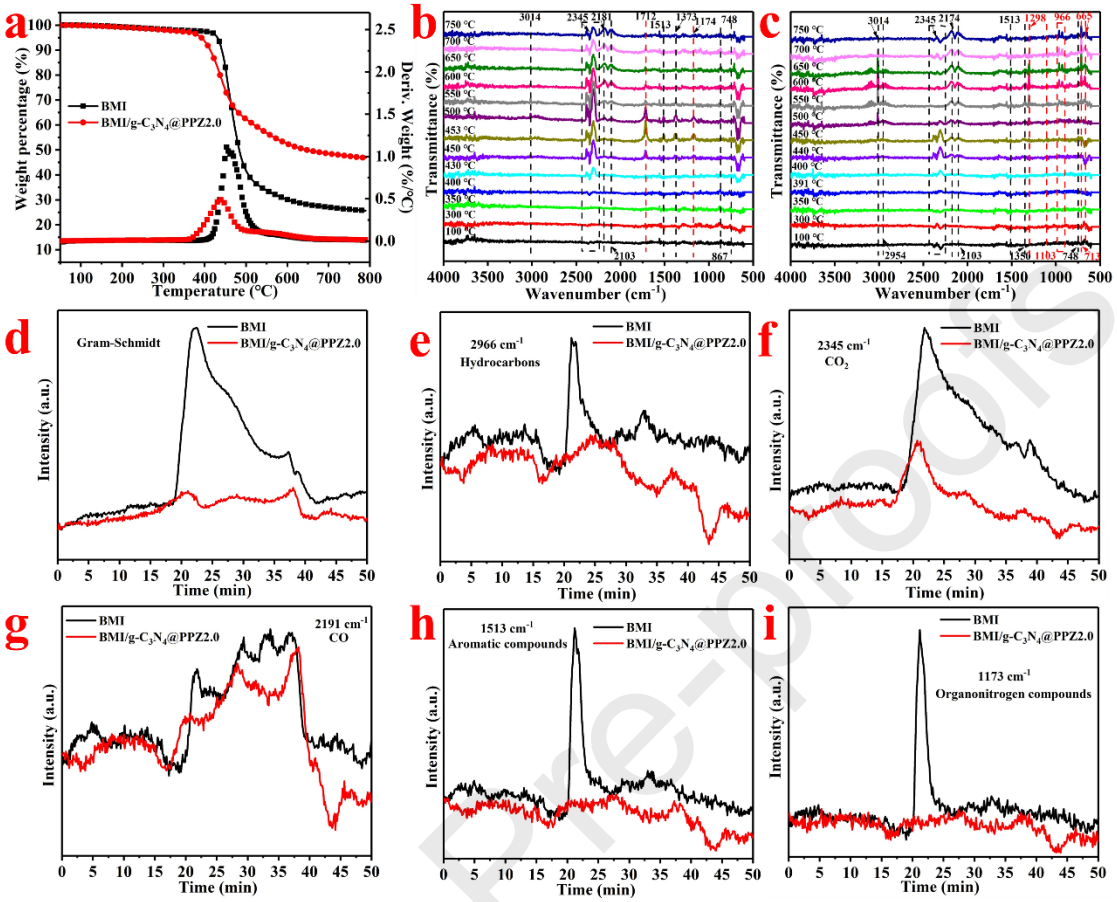

Fig.7 TGA (left Y coordinate) and DTG (right Y coordinate) curves of pure BMI, BMI/g-C_3N_4@PPZ2.0 in TG-FTIR test (a); FT-IR spectra of pure BMI, BMI/g-C_3N_4@PPZ2.0 at different pyrolysis temperatures (b-c); Absorbance of pyrolysis products versus time curves of pure BMI, BMI/g-C_3N_4@PPZ2.0: total pyrolysis products (d), hydrocarbons (e), CO_2 (f), CO (g), aromatic compounds (h) and organonitrogen compounds (i), respectively.

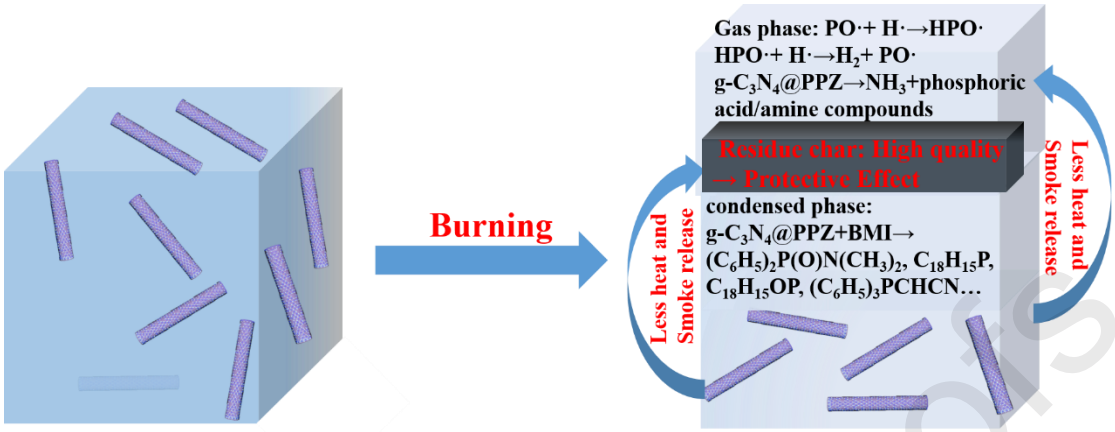

Scheme 2. Schematic illustration of flame-retardant mechanism for g-C_3N_4@PPZ in BMI composites.

Journal Pre-proofs

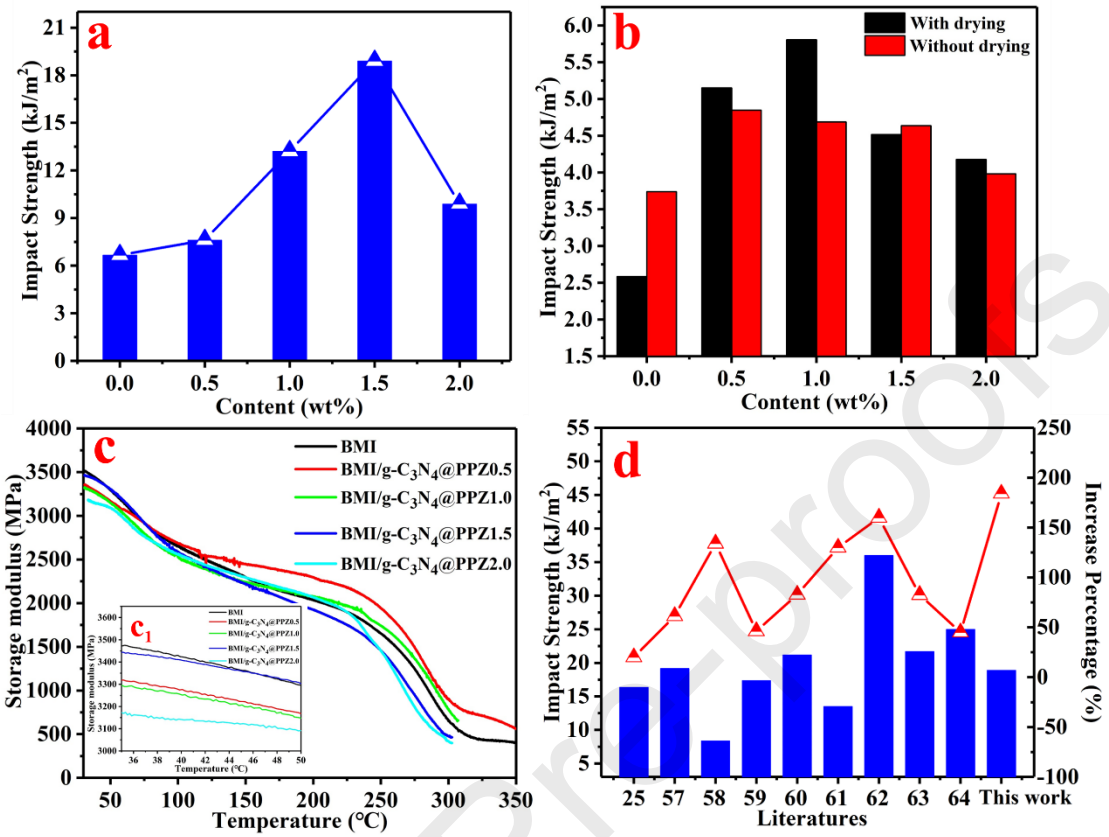

Fig.8 The impact strength results of pure BMI and BMI composites in normal and damp-humid conditions (a-b); the storage modulus (E′) results of BMI and BMI composites obtained by DMA test (c); the comparison of impact strength (left Y coordinate) and improvement efficiency (right Y coordinate) with other bismaleimide systems in the literatures (d).

Journal Pre-proofs

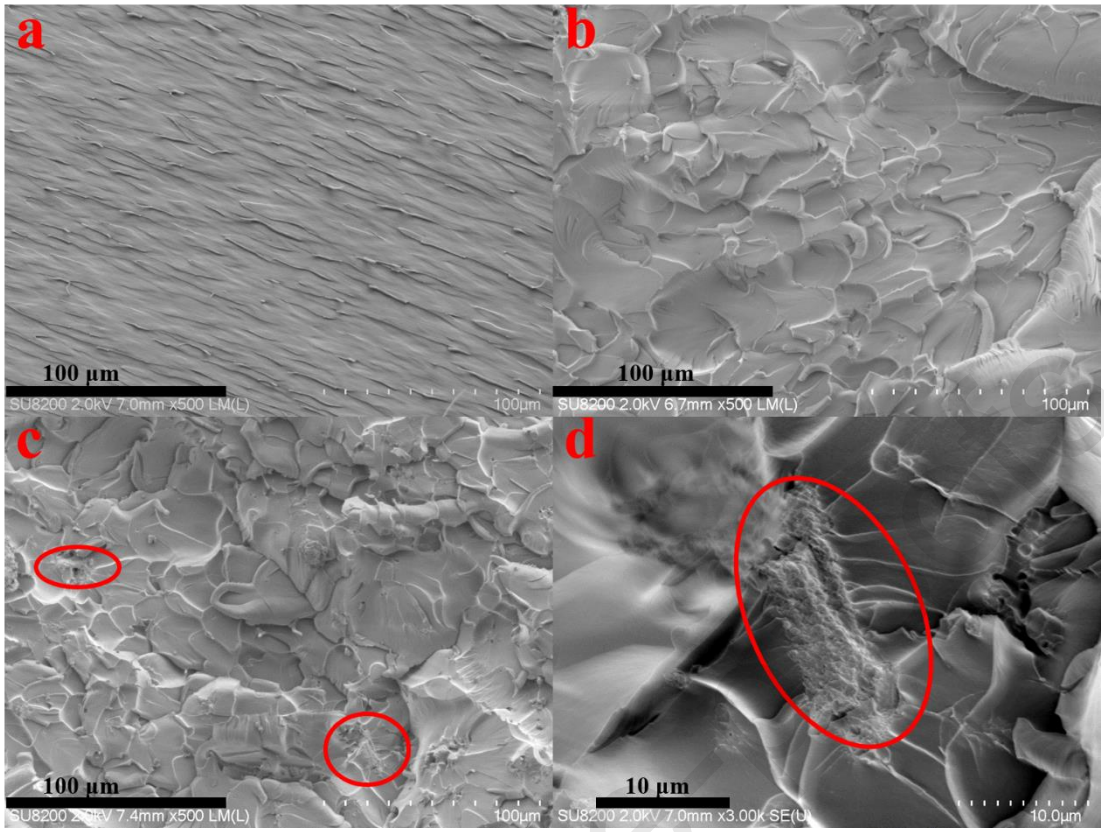

Fig.9 The SEM images of impact fracture surface of pure BMI (a) and BMI/g-C_3N_4@PPZ1.5 (b) and BMI/g-C_3N_4@PPZ2.0 (c-d) composites.

Journal Pre-proofs

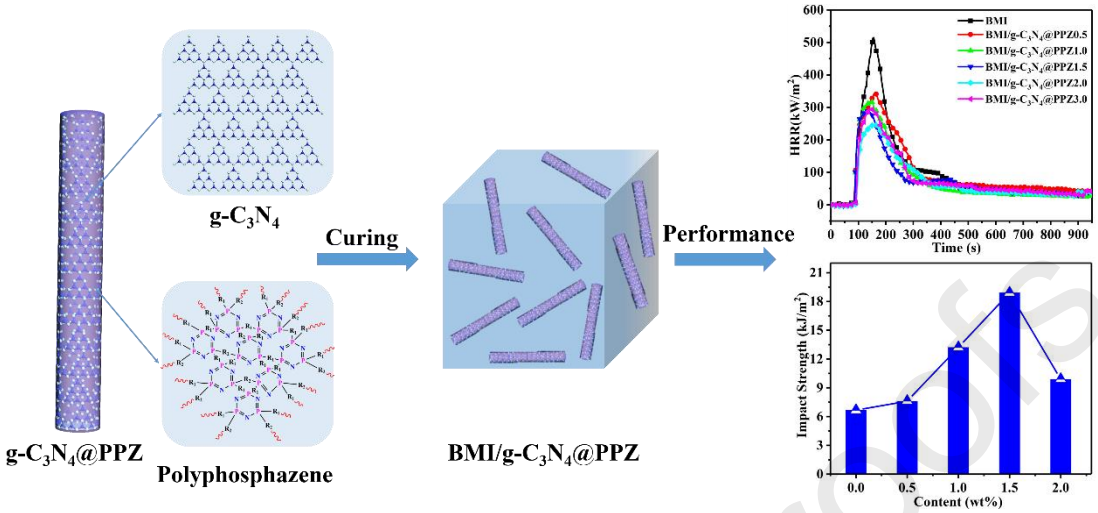

Table of Contents Graphic

Highlights

1. Innovation: novel g-C_3N_4@PPZ to promote flame retardant and toughness of BMI.
2. High-efficiency: PHRR and TSPR of BMI/g-C_3N_4@PPZ2.0 reduced by 52.1%, 53.8%.
3. The best impact strength of BMI/g-C_3N_4@PPZ increased by 184.0%.
4. Mechanism: the flame retardant and toughening mechanism was proposed.

Declaration of Interest Statement

The authors declare no competing financial interest.

Journal Pre-proofs